Song Jiyun (Orcid ID: 0000-0002-9483-0501)
Wang Zhi-Hua (Orcid ID: 0000-0001-9155-8605)
Wang Chenghao (Orcid ID: 0000-0001-8846-4130)

The Regional Impact of Urban Heat Mitigation Strategies on Planetary Boundary-Layer Dynamics over a Semi-arid City

Jiyun Song[1,2,3,*], Zhi-Hua Wang[1], and Chenghao Wang[1]

[1]School of Sustainable Engineering and the Built Environment, Arizona State University, Tempe, AZ 85287, USA.

[2]Department of Applied Mathematics and Theoretical Physics, Centre for Mathematical Sciences, University of Cambridge, Wilberforce Road, Cambridge, CB3 0WA, UK.

[3]Department of Architecture, University of Cambridge, 1-5 Scroope Terrace, Cambridge, CB2 1PX, UK.

Corresponding author: Jiyun Song (jsong52@asu.edu)

Key Points:

- Green roofs have slightly greater cooling efficiency than white roofs for a semiarid city.
- Both roofs reduce PBL height over urban core but increase PBL height over urban outskirts.
- Both roofs reduce CAPE over urban core but increase CAPE over urban outskirts.

This is the author manuscript accepted for publication and has undergone full peer review but has not been through the copyediting, typesetting, pagination and proofreading process, which may lead to differences between this version and the Version of Record. Please cite this article as doi: 10.1029/2018JD028302

Abstract

The rapid urbanization and associated landscape changes strongly modulate heat and moisture transfer processes on the urban surface as well as in the planetary boundary layer (PBL) via urban land-atmosphere interactions. In this study, we employed the mesoscale Weather Research and Forecasting (WRF) model with realistic urban dynamics to assess the effects of two urban landscaping strategies for urban heat mitigation (viz. green roofs and white roofs) on the PBL dynamics for hot summer periods over a semi-arid city, Phoenix of Arizona. Our results show that the effects of green roofs and white roofs on PBL dynamics are markedly different at daytime and nighttime. At daytime, both roofing systems reduce the sensible heat flux significantly by ~150 Wm^{-2}, lower the PBL height by ~700 m, and decrease the maximum convective available potential energy (CAPE) by ~40 Jkg^{-1} over the built terrain. At nighttime, both sensible and latent heat fluxes increase with green roofs by ~4 Wm^{-2} and ~6 Wm^{-2}, respectively. In contrast, with white roofs, a marginal reduction of sensible heat flux by ~4 Wm^{-2} was observed, owing to the remnant effect of daytime cooling. In addition, both roofing systems reduce the CAPE over the urban core but increase the CAPE over the rural surrounding, implying that the use of green or white roofs may potentially enhance the probability of precipitation towards the outskirt of the city.

Keywords: *Semi-arid city*; *Planetary boundary layer dynamics*; *Urban heat mitigation*; *Convective available potential energy*; *Green roof*; *White roof*

1 Introduction

The past decades have seen rapid urbanization globally, resulting in significant modifications on the land surfaces. The conversion of natural to built-up areas, with a larger fraction of man-made infrastructure and less vegetation and soil cover, in turn, alters the surface thermal and hydrological processes (Burian & Shepherd, 2005; Grimmond, 2007; Oleson et al., 2011). For example, dense building arrays induce complex radiative shading and trapping processes in the street canyon and influence the urban wind flow pattern through the modification of surface roughness (Bornstein & Johnson, 1977; Oke 1982; Fernando, 2010; Dou et al., 2014). In addition, the lack of natural surfaces (vegetation or soil) leads to repartition of the available energy into more sensible but less latent heat fluxes, and the modification of hydrological cycle including the decrease of evapotranspiration, infiltration, and groundwater recharge, as well as the increase of surface runoff volume and rate (Burian & Shepherd, 2005). The large thermal mass of man-made infrastructure compounded by reduced vegetation evapotranspiration and excessive greenhouse gas emissions due to intensive human activities in urban areas could lead to higher surface and air temperatures in urban areas when compared with surrounding rural areas, known as the urban heat island (UHI) effect (Landsberg, 1981; Oke, 1982). In addition to the UHI effect, extreme heat events associated with heat waves bring great health risks and more cooling energy demand to urban populations (Grimmond, 2007).

To combat UHI and the concomitant environmental challenges, many urban heat mitigation strategies have been proposed and evaluated by researchers and adopted by city planners, such as the implementation of green infrastructure (e.g. urban lawn, tree, green roof) and reflective material (e.g. cool pavement, white roof) (Akbari et al., 2001; Santamouris, 2014; Takebayashi & Moriyama, 2007; Chow et al., 2012). Previous research mainly focused on assessing the impact of urban heat mitigation strategies on the urban surface or near-surface conditions such as surface temperature, 2-meter air temperature, pedestrian thermal comfort, and building energy consumption (Georgescu et al., 2011; Sailor et al., 2011; Shashua-Bar et al., 2011; Yang et al., 2016). These impact of modified urban surface hydrothermal processes, in turn, will be manifest in the planetary boundary layer (PBL), leading to changes in local and regional hydroclimates via land–atmosphere interactions (Georgescu, 2015; Sharma et al., 2016; Song and Wang, 2016). Despite its importance, urban-induced changes in PBL dynamics have been under-explored up to date.

One of the typical urban-induced regional climate change phenomena is the modified convective precipitation pattern, which are mainly due to spatiotemporal variability of the UHI intensity and the convective available potential energy (CAPE) (Bornstein & Lin, 2000; Burian & Shepherd, 2005; Zhang et al., 2009; Dou et al., 2014). Numerous studies found that warm-season precipitations significantly increase over and downwind of major cities as a result of the UHI-induced convective activity and the UHI-enhanced surface convergence (Huff & Changnon, 1972, 1973; Bornstein & Lin, 2000; Shepherd et al., 2002; Burian & Shepherd, 2005). On the other hand, precipitations over built-up and downwind areas could decrease, as a consequence of

less moisture availability and the formation of deeper boundary layers; both are related to the reduction of CAPE (Bornstein & LeRoy, 1990; Guo et al., 2006; Zhang et al., 2009).

With the implementation of urban heat mitigation strategies at city scale, urban surface heat and moisture transfer processes will be further modified, which will in turn modulate the overlying PBL dynamics (e.g. the intensity of UHI, the patterns of CAPE, the possibility of urban-induced precipitation). The objective of this study is to better understand the impact of urban heat mitigation strategies on the PBL dynamics through the mesoscale Weather Research and Forecasting (WRF) model simulations. A rapidly growing semi-arid city, viz. the Phoenix metropolitan area in Arizona, USA, is selected as our testbed. The metropolitan Phoenix has undergone tremendous urban growth during the past decades and experienced strong heat stress with continuously increasing UHI intensity in this area (Chow et al., 2012; Wang et al., 2016; Song et al., 2017). In this study, we will evaluate two particular urban heat mitigation strategies, i.e. green (vegetated) and white (reflective or "cool") roofs. Both green and white roofs can alter the urban surface energy balance by repartitioning the available energy (Akbari et al., 2001; Takebayashi & Moriyama, 2007; Coutts et al., 2013; Georgescu, 2015; Solcerova et al., 2017). In addition, green roofs in arid or semi-arid environments also modify urban hydrological processes via irrigation and water retention. The results of this study could help us to answer the following research questions, including "Which urban heat mitigation strategy is more sustainable for Phoenix city? Green or white roof?", "What is the spatiotemporal variability of PBL dynamics induced by green and white roofs?", and "What are the implications of urban landscape modifications on local and regional hydroclimate?".

2 Methodology

2.1 Parameterization of urban surface energy and water budgets

To better capture the transport of surface energy and water budgets in a built environment, we adopted the latest single-layer urban canopy model (SLUCM) with a realistic urban hydrological model, developed by Wang et al. (2013) and integrated into the WRF platform (Yang et al., 2015, 2016). This SLUCM not only captures the surface heterogeneity in the built environment but also incorporates complex urban vegetation dynamics and hydrological processes such as urban irrigation. The total turbulent sensible and latent heat fluxes arising from urban surface (H_s and LE_s) are the summations of the areal-proportional fluxes from different urban facets (i.e. roofs, walls and grounds), namely

$$H_s = r\sum_{k=1}^{N_R} f_{R,k}H_{R,k} + 2h\sum_{k=1}^{N_W} f_{W,k}H_{W,k} + w\sum_{k=1}^{N_G} f_{G,k}H_{G,k}\,, \tag{1}$$

$$LE_s = r\sum_{k=1}^{N_R} f_{R,k}LE_{R,k} + 2h\sum_{k=1}^{N_W} f_{W,k}LE_{W,k} + w\sum_{k=1}^{N_G} f_{G,k}LE_{G,k}\,, \tag{2}$$

where H and LE are sensible and latent heat fluxes respectively for a generic surface, N is the number of sub-facets on each facet, f is the areal fraction of each sub-facet, with the subscripts R, W, G denoting roof, wall, and ground respectively; r, h, and w are the normalized dimensionless roof width, building height, and street width respectively. The H_s and LE_s predicted by the SLUCM then provide the lower boundary condition for the PBL turbulence simulation, namely

$$\overline{\left(w'\theta'\right)_s} = \frac{H_s}{\rho_a c_p}, \tag{3}$$

$$\overline{\left(w'q'\right)_s} = \frac{LE_s}{\rho_a L_v}, \tag{4}$$

where θ is the potential temperature of air, q is the specific humidity of air, ρ_a is the density of air, c_p is the heat capacity of air, L_v is the latent heat of vaporization of water, the subscript "s" denotes the surface condition, and the superscript (i.e. the prime symbol) denotes the turbulent fluctuation.

2.2 Parameterization of PBL dynamics

To predict dynamics of the PBL, the WRF-Yonsei University (YSU) PBL scheme (Noh et al., 2003; Hong et al., 2006; Hong, 2010) is used in this study. The YSU PBL scheme is a first-order nonlocal closure method, which has been widely used in numerical weather predictions, well evaluated under different stability conditions and better in predicting the convective boundary layer than local closure schemes (Bright & Mullen, 2002; Pagowski, 2004; Hu et al., 2013; Shin & Hong, 2011). More specifically, the YSU scheme is a modified K-profile model, which considers the effects of non-local mixing and entrainment/inversion (Hong et al., 2006; Hong, 2010). The governing equation for prognostic variables X (such as zonal wind, meridional wind, potential temperature, specific humidity, cloud water mixing ratio, cloud ice mixing ratio, etc.) can be expressed by

$$\frac{\partial X}{\partial t} = \frac{\partial}{\partial z}\left\{K_c\left(\frac{\partial X}{\partial z} - \gamma_c\right) - \overline{\left(w'X'\right)_h}\left(\frac{z}{h}\right)^3\right\}, \tag{5}$$

where t is time, z is the model height, K_c is the eddy diffusivity coefficient, γ_c is a non-local counter-gradient term as a correction to the local gradient which incorporates the contribution of large-scale eddies to the total flux, h is the PBL height, $\overline{\left(w'X'\right)}$ is the ensemble averaged vertical kinematic eddy flux, with the subscript h denoting the flux is at the PBL height (i.e. at the inversion layer).

In particular, the PBL height is a key indicator of the PBL structure, which is defined as the vertical level where the continuous turbulent flux vanishes and is determined by (Troen & Mahrt, 1986)

$$h = \frac{Ri_{Bc} U^2}{\beta \Delta \theta_v}, \tag{6}$$

where Ri_{Bc} is the critical bulk Richardson number, β is the buoyancy parameter, i.e. $\beta = g/T_0$, where g is the acceleration due to gravity, and T_0 is the reference temperature, U is the horizontal wind speed at PBL height, and $\Delta\theta_v$ is the difference of virtual potential temperatures between the PBL height and the surface level. Another important indicator of PBL dynamics is the convective available potential energy (CAPE), which manifests the atmospheric instability and the potential density of deep convection and has been widely used in convective precipitation prediction, severe weather analysis and forecasting, cumulus parameterization in general circulation models, etc. (Washington & Parkinson, 2005; Donner & Phillips, 2003; Meukaleuni et al., 2016). Previous observational studies show that the variability of the CAPE is largely dominated by PBL thermodynamic properties (McBride & Frank, 1999, Donner & Phillips, 2003; Zhang, 2009). Numerically, CAPE is the positive buoyancy of an air parcel calculated by integrating the local buoyancy of an air parcel vertically from the level of free convection (LFC) to the level of neutral buoyancy (LNB):

$$\text{CAPE} = \int_{P_{\text{LFC}}}^{P_{\text{LNB}}} R_d \left(T_{v,p} - T_{v,e} \right) d \ln p \,, \tag{7}$$

where p is the pressure of the air parcel; R_d is the gas constant for air, $T_{v,p}$ and $T_{v,e}$ are the virtual temperatures of the air parcel and the environment respectively. The virtual temperature T_v of a moist air parcel is the temperature that the dry air parcel would have with the same pressure and density (Stull, 1988), calculated as

$$T_v = T \frac{1 + r/\varepsilon}{1 + r}, \tag{8}$$

where T is the absolute temperature, r is the mixing ratio, and ε is the ratio of dry air to water vapor gas constants (ε = 0.622).

2.3 Numerical experimental setup

As a desert city in Arizona's Sun Corridor, Phoenix suffers severe heat stress with possible maximum temperature exceeding 50 °C in summer and is very vulnerable to climate-induced water shortages with an average annual precipitation of 203 mm among which the heaviest rainfall events usually occur in summer monsoon seasons (Andrade & Sellers, 1988; Karnieli & Osborn, 1988; Balling & Gober, 2007; Gober & Kirkwood, 2010; Song et al., 2017). The projected urban population growth and continuous trend of urban warming (Wang & Wang, 2017) will, in turn, lead to persistent stress in the repercussions of energy–water–climate nexus. It is therefore of crucial importance for the city to find sustainable strategies to mitigate urban heat and water stresses under the challenges of the future expansion and climate change;

innovative (reflective or vegetated) roofing systems are among the popular solutions in the region (Simpson & McPherson, 1997; Jo et al., 2010; Song & Wang, 2016; Yang et al., 2016).

In this study, we will focus on examining the impact of two popular urban heat mitigation strategies, i.e. green and white roofs on the PBL dynamics in summer for Phoenix metropolitan area based on WRF simulations. A nested grid configuration with three domains centered at Phoenix is presented in Fig.1, with the spatial resolution of 32, 8, and 2 km for the outer, middle, and inner domains, respectively. The MODIS global land cover data (Friedl et al., 2002) were used for the outer and middle domains, while the National Land Cover Database (NLCD) 2006 data (Fry et al., 2011) with a more detailed representation of urban land use variety were used for the inner domain. The input parameters of the WRF-urban modeling system for Phoenix metropolitan area are presented in Table 1. The gridded reanalysis data from the National Centers for Environmental Prediction Final (NCEP FNL) Operational Model Global Tropospheric Analyses were retrieved as the large-scale meteorological forcing from the National Center for Atmospheric Research (NCAR) Computational and Information Systems Laboratory Research Data Archive. Specifically, the large-scale meteorological data from 25 May to 31 August in 2012 were used to drive the WRF model, with the first week from 25 May to 31 May as the spin-up period and the 3 summer months from 1 June to 31 August (JJA) as the analysis period.

Three sets of simulations have been carried out for the selected summer period (JJA), including one control scenario with original urban landscapes, and two designed scenarios with modified landscapes. The two designed scenarios include (1) a green roof scenario by changing all the conventional roofs to green roofs with regular irrigation at 9 pm every day so that the function of green roof will not be limited by water availability, and (2) a white roof scenario by increasing all the roof albedo from 0.2 (conventional roof albedo) to 0.6 (a reasonable white roof albedo considering the long-term outwearing effect, ref: Santamouris, 2014; Yang et al., 2015). Note that during the irrigation, the volumetric moisture of the top two soil layers of green roofs in the model is set to reach the saturated volumetric moisture. Furthermore, the PBL dynamics are characteristically different at daytime and nighttime, namely daytime PBL is convectively unstable and well-mixed due to strong turbulence induced by uprising thermals, while nighttime PBL is convectively stable and stratified as the land surface cools down (Stull, 1988). Therefore, to assess the effects of different roofing strategies on PBL dynamics at daytime and nighttime, the differences of four PBL variables (H_s, LE_s, PBL height, maximum CAPE) between the control scenario and the design scenarios were averaged over the JJA period at 2 pm and 2 am local time respectively.

2.4 Model evaluation

To evaluate the model capacity, we compared the simulation results of surface fluxes (Fig. 2) and PBL profiles (Fig. 3) against the measurements under the control scenario. In Fig. 2, simulated surface sensible and latent heat fluxes (H_s and LE_s) were compared with the

measurements from an eddy covariance tower located at west Phoenix site (33°29'1.9" N, 112°08'33.4" W) in the pre-monsoon period from 13 June to 29 June, 2012. In Fig. 3, simulated vertical profiles of potential temperature (θ) and dewpoint temperature (T_d) were compared against experimental data at east Phoenix site (33°27' N, 111°57' W) obtained from the NOAA/ESRL radiosonde database (http://esrl.noaa.gov/raobs/) for two days (i.e. 24–25 June, 2012) in the pre-monsoon period. Simulations and measurements have good agreements with the root-mean-square error (RMSE) of 28.3 and 14.5 Wm^{-2} for H_s and LE_s respectively and mean RMSE of 1.6 K and 7.8 °C for θ and T_d from surface to 20,000 m, indicating that the model framework has the capability to predict reasonable surface states and PBL states.

3 Results and Discussions

The spatial variations of urban surface energy budgets (i.e. sensible and latent heat fluxes) at daytime (2 pm) induced by green roofs and white roofs are shown in Fig. 4a & b and Fig. 5a & b respectively. Within the urban core at daytime, green roofs and white roofs could reduce mean surface sensible heat fluxes by ~170 Wm^{-2} (Fig. 4a) and ~140 Wm^{-2} (Fig. 5a) respectively. This is expected as a result of the reduced urban surface temperatures: green roofs via evapotranspirative cooling and white roofs via reflection of shortwave radiation. It is also found that green roofs are slightly more effective than white roofs to reduce sensible heat flux by additional 30 Wm^{-2}, conditioned on the well-irrigated roof vegetation with additional uprising surface latent heat flux of ~10 Wm^{-2} (Fig. 4b). On the other hand, for most part of the surrounding rural areas, the daytime sensible heat flux will increase by ~20 Wm^{-2} in both green and white roof scenarios (Fig. 4a & Fig. 5a), possibly due to the enhanced surface heat flux divergence from urban to rural area induced by subsidence on the periphery of urban area (Oke, 1976, 1982; Oke et al., 2017). In addition, we found a comparatively large increase of daytime latent heat flux (~20 Wm^{-2}) over the northern and northeastern parts in both roof scenarios (Fig. 4b & Fig. 5b). This is probably caused by an enhanced surface divergence of moisture induced by the topographical effect since the northern and northeastern parts of the domain are mainly high-elevation terrain covered by national forests (see Fig.1a & b). In contrast to the daytime condition, the effects of both roofs are less significant at nighttime with a minor difference of ±4 Wm^{-2} and ±3 Wm^{-2} for sensible heat flux (Fig. 6a & Fig. 7a) and latent heat flux (Fig. 6b & Fig. 7b) respectively. The less magnitude of changes in nocturnal energy budgets is anticipated owing to the limited total available energy during nighttime.

Since the PBL dynamics are strongly regulated by the heat and moisture transport processes on land surfaces (Chen & Avissar, 1994; Flagg & Taylor, 2011; Song & Wang, 2015; Sharma et al., 2016), the changes of surface sensible and latent heat fluxes necessarily lead to the changes of PBL states such as the PBL height and the CAPE. We found that the daytime PBL height significantly decreases over the urban area by about 700 m and slightly increases over most parts of rural areas by about 100 m in both green and white roof scenarios (see Fig. 4c & Fig. 5c). Besides, the daytime maximum CAPE is reduced by about 40 Jkg^{-1} over the urban core and increased by about 40 Jkg^{-1} over the surrounding rural area in both roof scenarios (see Fig.

4d & Fig. 5d). The decrease of daytime PBL height and CAPE over the urban area is possibly owed to the reduction of vertical mixing, buoyant energy, and convective rolls as a result of the decreased uprising urban surface sensible heat flux, vice versa for the surrounding rural area (Blanchard, 1998). On the other hand, we found that the effects of both roofing strategies on PBL height over urban areas are less significant at nighttime (with ±30 m difference) than at daytime (with 700 m difference). Although the nocturnal PBL height variation is not monotonous over the entire urban environment in the study area, in general, green roofs tend to reduce PBL height (Fig. 6c) and white roofs behave otherwise (Fig. 7c). In addition, we noticed a relatively prominent decrease of the maximum nighttime CAPE (15~20 Jkg^{-1}) over the urban area and a relatively prominent increase of the maximum nighttime CAPE (20 Jkg^{-1}) at some peripheral rural parts in both scenarios (Fig. 6d & 7d), although increased CAPEs occur at different rural locations (the southern part for green roof scenario and the western part for white roof scenario).

These results have important implications for the urban heat mitigation, urban air quality, and urban convective rainfall initiation. First of all, both green and white roofs could help mitigate the daytime UHI by reducing sensible heat fluxes in the urban area. Although green roofs (under current model settings with regular irrigation) are found to be slightly more effective than white roofs in reducing an additional sensible heat flux of 30 Wm^{-2}, the cooling effectiveness of green roofs is largely influenced by soil moisture and requires large amounts of water to maintain (Coutts et al., 2013; Solcerova et al., 2017). A rough estimate of annual water demand for irrigation in a total green roof scenario would be about 3.62×10^8 m^3, which are about 4 times more than the current condition without green roof (0.77×10^8 m^3) (Yang and Wang, 2017). According to Arizona Department of Water Resources (2010, 2014), average annual municipal water demand in the Phoenix metropolitan area is about 15.59×10^8 m^3 in the period 2001-2005 and will be increased by 0.46~1.21×10^8 m^3 in the period 2006-2025. An additional annual water demand for green roof irrigation (2.85×10^8 m^3) would be about 17% of the average annual municipal water demand (16×10^8 m^3), bringing more stress to the water resources supply for a semi-arid city. Therefore, the choice of heat mitigation strategies (green or white roofs) in the study area is conditioned on complex trade-offs in the energy–water–ecosystem-service nexus, calling for a comprehensive life cycle analysis on the total environmental benefits as an imperative future research need.

Secondly, due to the effects of local topography and intensive anthropogenic emissions, the air quality over the urban core of Phoenix is usually worse than that over urban outskirts. Both roofing strategies might result in even worse air quality over the urban core at daytime because air pollutants tend to stagnate in the PBL with higher concentration resulting from reduced vertical turbulent mixing and shrunken PBL depth. However, the impact of green roofs on urban air pollution is more complicated than white roofs, since it can not only regulate the PBL dynamics but also remove air pollutants via both dry and wet depositions (Wang et al., 2017). In addition, both roofing strategies might influence the regional precipitation patterns by suppressing the growth of the daytime urban PBL, altering the spatial distribution of surface

fluxes, modifying the atmospheric moisture advection, and affecting the convective precipitation initiation. In particular, since the CAPE implies the available potential buoyancy to lift an air parcel and dominates the genesis and intensity of convective precipitation (Riemann-Campe et al., 2009), decreased CAPE over the urban core and increased CAPE over the surrounding suburban area might imply that convective precipitation has a higher possibility to initiate at suburban areas. For example, the increases of latent heat flux and CAPE over the northeastern forest area under both roof scenarios can probably lead to more daytime convective precipitation potential and more regional moisture flux divergence due to topographical effects (Fig. 5b & d, Fig. 6b & d).

To better investigate the relationship between CAPE and precipitation in Phoenix area, we further analyzed the trend of the maximum CAPE during two rainfall events, including a daytime rainfall event on 04 July 2012 and a nighttime rainfall event on 21–22 August 2012 as shown in Fig. 8a & b respectively. For both daytime and nighttime cases, the CAPE increased before the rainfall event and decreased after the rainfall event, resulting in the largest value at the beginning of the rainfall event. Since CAPE is a prerequisite for convection, increases of CAPE might result in higher possibilities of convective rainfall initiation and greater precipitation totals (DeMott & Randall, 2004). On the other hand, the rainfall activity might in turn destroy the convective atmospheric structure, restrain the increase of buoyant energy and reduce CAPE. Since the local precipitation is not only influenced by the local-scale surface forcing, atmospheric moisture availability, aerosols, and cloud condensation nuclei, but also by large-scale atmospheric advections (Yang et al., 2014; Oke et al., 2017), the correlation between CAPE and precipitation amount still remains unclear (Blanchard, 1998, DeMott & Randall, 2004). It could be constructive and informative to investigate the sole impact of two CAPE sub-terms, i.e. the buoyancy and the integration depth from LFC to LNB, on precipitation in the future. For instance, the normalized CAPE value (i.e. CAPE divided by the integration depth) might serve as a more useful indicator of the convective updraft strength, especially for environments with shallow LFCs and small CAPEs such as in Phoenix city. In addition, more observation data of precipitation and the corresponding CAPE at different weather stations need to be analyzed to gain a more realistic relationship between CAPE and precipitation amount over the study area.

4 Concluding Remarks

In this study, we evaluated the impact of green roof and white roof on PBL dynamics (including surface heat fluxes, the PBL height, and the CAPE) over the Phoenix metropolitan area using a mesoscale WRF-urban modeling system. We found that generally the impact of green roofs and white roofs on PBL is less significant at nighttime than at daytime, possibly due to the limited total available energy in the absence of solar radiation. Both green and white roofs are effective in the UHI mitigation by significantly reducing the surface sensible heat flux (by

~150 Wm^{-2}). In addition, both roofs would lead to possible urban air quality deterioration, since reduced uprising thermals, weakened vertical mixings, and shrunken PBL depths are disadvantages for urban pollutant dispersion. In contrast to white roofs, green roofs can add extra moisture to the PBL with additional latent heat fluxes and remove air pollutants through dry and wet depositions, but require a large amount of water for regular irrigation to maintain cooling effectiveness and plant activity, which is another challenge for a semi-arid city. Therefore, there is not a simple answer to the question "which roofing strategy is more sustainable for Phoenix city" considering the complex trade-offs in the energy–water–ecosystem-service nexus. Furthermore, both roofs will lead to decreased maximum CAPE in the urban core and increased maximum CAPE over urban outskirts at either daytime or nighttime. The spatial variation of the CAPE implies that the local landscape change can possibly affect the regional precipitation pattern through land–atmosphere interactions. For example, with the implementation of green roofs, although more atmospheric moisture is available, the convective precipitation initiation will be suppressed over the urban core with less thermal uplifting energy, but enhanced over the urban–rural fringe and the northeastern forest.

Note that the spatiotemporal variability of the simulated scenarios was sampled at two particular local time instants (viz. 2 am and 2 pm) in this study, without presenting the detailed vertical distribution and diurnal variation of PBL variables. The effect on convective precipitation can be refined with cloud microphysics (e.g. cloud cover and cloud height) retrieved from satellites and ground-based radars. In addition, resolving the real-time interaction between urban boundary layer meteorology and air pollution is highly recommended for future model development. Nevertheless, this study presents a step forward by assessing the impact of green and white roofs on the PBL (from the surface to several kilometers high), while most previous work only focused on near-surface atmospheric dynamics, such as surface temperature or 2-m air temperature. The results of this study are expected to be informative for city planners and stakeholders in Phoenix, Arizona and other arid/semi-arid cities, while the extension to cities in different geographical, climatic, and socio-economic conditions needs to be caveated.

Acknowledgments

This work is mainly supported by U.S. National Science Foundation (NSF) under the Urban Sustainability program (grant # CBET-1435881). J. Song is currently supported by two EPSRC grants in U.K.: Managing Air for Green Inner Cities (MAGIC) (EP/N010221/1) and Low Carbon Climate-responsive Heating and Cooling of Cities (LoHCool) (EP/N009797/1). The NCAR/CISL supercomputing resources used for model simulation and analysis are greatly acknowledged. The large-scale forcing used in this study, i.e. the gridded reanalysis data from the National Centers for Environmental Prediction Final (NCEP FNL) Operational Model Global Tropospheric Analyses, can be retrieved from the National Center for Atmospheric Research (NCAR) Computational and Information Systems Laboratory Research Data Archive (http://rda.ucar.edu/datasets/ds083.2/#access). The observation data used for model validation can be obtained from Central Arizona–Phoenix Long-Term Ecological Research

(CAPLTER)database (https://sustainability.asu.edu/caplter/data/) and NOAA/ESRL radiosonde database (http://esrl.noaa.gov/raobs/).

References

Akbari, H., Pomerantz, M., & Taha, H. (2001). Cool surfaces and shade trees to reduce energy use and improve air quality in urban areas. *Solar Energy*, *70*(3), 295-310. http://doi.org/10.1016/S0038-092X(00)00089-X.

Andrade, E. R., & Sellers, W. D. (1988). El Niño and its effect on precipitation in Arizona and western New Mexico. *International Journal of Climatology*, *8*(4), 403-410. http://doi.org/10.1002/joc.3370080407.

Arizona Department of Water Resources (2010). Fourth management plan. Retrieved from: http://www.azwater.gov/AzDWR/WaterManagement/AMAs/FourthManagementPlan.htm.

Arizona Department of Water Resources (2014). AMA Cultural Water Demand – Municipal Demand, (http://www.azwater.gov/azdwr/StatewidePlanning/WaterAtlas/ActiveManagementAreas/PlanningAreaOverview/CulturalWaterDemand-Municipal.htm).

Balling Jr, R. C., & Gober, P. (2007). Climate variability and residential water use in the city of Phoenix, Arizona. *Journal of Applied Meteorology and Climatology*, *46*(7), 1130-1137. http://doi.org/10.1175/JAM2518.1.

Blanchard, D. O. (1998). Assessing the vertical distribution of convective available potential energy. *Weather and Forecasting*, *13*(3), 870-877. http://doi.org/10.1175/1520-0434(1998)013<0870:ATVDOC>2.0.CO;2.

Bornstein, R.D., & Johnson, D.S. (1977). Urban-rural wind velocity differences. Atmospheric Environment, 11(7), 597-604. https://doi.org/10.1016/0004-6981(77)90112-3.

Bornstein, R., & LeRoy, M. (1990). Urban barrier effects on convective and frontal thunderstorms. Preprint volume, Fourth AMS Conference on Mesoscale Processes, Boulder, CO, 25-29 June.

Bornstein, R., & Lin, Q. (2000). Urban heat islands and summertime convective thunderstorms in Atlanta: three case studies. *Atmospheric Environment*, 34, 507-516. https://doi.org/10.1016/S1352-2310(99)00374-X.

Bright, D. R., & Mullen, S. L. (2002). The sensitivity of the numerical simulation of the southwest monsoon boundary layer to the choice of PBL turbulence parameterization in MM5. *Weather and Forecasting*, *17*(1), 99-114. https://doi.org/10.1175/1520-0434(2002)017<0099:TSOTNS>2.0.CO;2.

Burian, S. J., & Shepherd, J. M. (2005). Effect of urbanization on the diurnal rainfall pattern in Houston. *Hydrological Processes*, 19, 1089-1103. https://doi.org/10.1002/hyp.5647.

Chen, F., & Avissar, R. (1994). Impact of land-surface moisture variability on local shallow convective cumulus and precipitation in large-scale models. *Journal of Applied Meteorology*, *33*(12), 1382-1401. https://doi.org/10.1175/1520-0450(1994)033<1382:IOLSMV>2.0.CO;2.

Chen, F., Kusaka, H., Bornstein, R., Ching, J., Grimmond, C.S.B., Grossman-Clarke, S., Loridan, T., Manning, K.W., Martilli, A., Miao, S.G., Sailor, D., Salamanca, F.P., Taha, H., Tewari, M.,Wang, X.M.,Wyszogrodzki, A.A., & Zhang, C.L. (2011). The integrated WRF/urban

modelling system: development, evaluation, and applications to urban environmental problems. *International Journal of Climatology*, 31, 273–288, https://doi.org/10.1002/joc.2158.

Chow, W. T., Brennan, D., & Brazel, A. J. (2012). Urban heat island research in Phoenix, Arizona: Theoretical contributions and policy applications. *Bulletin of the American Meteorological Society*, *93*(4), 517-530. https://doi.org/10.1175/bams-d-11-00011.1.

Chow, W.T.L., Volo, T.J., Vivoni, E.R., Jenerette, G.D., & Ruddell, B.L. (2014). Seasonal dynamics of a suburban energy balance in Phoenix, Arizona. *International Journal of Climatology*, 34, 3863-3880, https://doi.org/10.1002/joc.3947.

Coutts, A. M., Daly, E., Beringer, J., & Tapper, N. J. (2013). Assessing practical measures to reduce urban heat: green and cool roofs. *Building and Environment*, 70, 266-276. https://doi.org/10.1016/j.buildenv.2013.08.021.

DeMott, C. A., & Randall, D. A. (2004). Observed variations of tropical convective available potential energy. *Journal of Geophysical Research: Atmospheres*, 109, D2. https://doi.org/10.1029/2003JD003784.

Donner, L. J., & Phillips, V. T. (2003). Boundary layer control on convective available potential energy: Implications for cumulus parameterization. *Journal of Geophysical Research: Atmospheres*, 108, D22. https://doi.org/10.1029/2003JD003773.

Fernando, H. J. S. (2010). Fluid dynamics of urban atmospheres in complex terrain. *Annual Review of Fluid Mechanics*, 42, 365-389. https://doi.org/10.1146/annurev-fluid-121108-145459.

Flagg, D. D., & Taylor, P. A. (2011). Sensitivity of mesoscale model urban boundary layer meteorology to the scale of urban representation. *Atmospheric Chemistry and Physics*, *11*(6), 2951-2972. https://doi.org/10.5194/acp-11-2951-2011.

Friedl, M. A., McIver, D. K., Hodges, J. C., Zhang, X. Y., Muchoney, D., Strahler, A. H., … Baccini, A. (2002). Global land cover mapping from MODIS: algorithms and early results. *Remote Sensing of Environment*, *83*(1), 287-302. https://doi.org/10.1016/S0034-4257(02)00078-0.

Fry, J. A., Xian, G., Jin, S., Dewitz, J. A., Homer, C. G., Yang, L., … Wickham, J. D. (2011). Completion of the 2006 national land cover database for the conterminous United States. *Photogrammetric Engineering & Remote Sensing*, *77*(9), 858-864.

Georgescu, M., Moustaoui M., Mahalov A., Dudhia J. (2011) An alternative explanation of the semiarid urban area "oasis effect". Climate and Dynamics, 116, D24. https://doi.org/10.1029/2011JD016720.

Georgescu, M. (2015). Challenges associated with adaptation to future urban expansion. *Journal of Climate*, 28(7), 2544-2563, https://doi.org/10.1175/JCLI-D-14-00290.1.

Gober, P., & Kirkwood, C. W. (2010). Vulnerability assessment of climate-induced water shortage in Phoenix. *Proceedings of the National Academy of Sciences*, *107*(50), 21295-21299. https://doi.org/10.1073/pnas.0911113107.

Grimmond, S. (2007). Urbanization and global environmental change: local effects of urban warming. *Cities and global environmental change*, 173(1), 83-88. https://doi.org/10.1111/j.1475-4959.2007.232_3.x.

Hong, S. Y., Noh, Y., & Dudhia, J. (2006). A new vertical diffusion package with an explicit treatment of entrainment processes. *Monthly Weather Review*, *134*(9), 2318-2341. https://doi.org/10.1175/MWR3199.1.

Hong, S. Y. (2010). A new stable boundary-layer mixing scheme and its impact on the simulated East Asian summer monsoon. *Quarterly Journal of the Royal Meteorological Society*, *136*(651), 1481-1496. https://doi.org/10.1002/qj.665.

Hu, X. M., Klein, P. M., & Xue, M. (2013). Evaluation of the updated YSU planetary boundary layer scheme within WRF for wind resource and air quality assessments. *Journal of Geophysical Research: Atmospheres*, 118, 18. https://doi.org/10.1002/jgrd.50823.

Jo, J. H., Carlson, J., Golden, J. S., Bryan, H. (2010). Sustainable urban energy: Development of a mesoscale assessment model for solar reflective roof technologies. *Energy Policy*, *38*(12), 7951-7959. https://doi.org/10.1016/j.enpol.2010.09.016.

Karnieli, A., & Osborn, H. B. (1988). Factors affecting seasonal and annual precipitation in Arizona. Hydrology and Water Resources in Arizona and the Southwest, 16 April 1988, 7, 18, Tucson, AZ, Arizona Section, American Water Resources Association, and the Hydrology Section, Arizona–Nevada Academy of Science.

Landsberg, H.E. (1981). The urban climate. Academic Press: New York, USA, 275 pp.

Meukaleuni, C., Lenouo, A., & Monkam, D. (2016). Climatology of convective available potential energy (CAPE) in ERA–Interim reanalysis over West Africa. *Atmospheric Science Letters*, *17*(1), 65-70. https://doi.org/10.1002/asl.601.

McBride, J. L., & Frank, W. M. (1999). Relationships between stability and monsoon convection. *Journal of the Atmospheric Sciences*, *56*(1), 24-36. https://doi.org/10.1175/1520-0469(1999)056<0024:RBSAMC>2.0.CO;2.

Myint, S.W., Gober, P., Brazel, A., Grossman-Clarke, S., & Weng, Q. (2011). Per-pixel vs. object-based classification of urban land cover extraction using high spatial resolution imagery. *Remote Sensing of Environment*, 115, 1145-1161, https://doi.org/10.1016/j.rse.2010.12.017.

Noh, Y., Cheon, W. G., Hong, S. Y., & Raasch, S. (2003). Improvement of the K-profile model for the planetary boundary layer based on large eddy simulation data. *Boundary-Layer Meteorology*, *107*(2), 401-427. https://doi.org/10.1023/A:1022146015946.

Oke T.R. (1976) The distinction between canopy and boundary-layer urban heat islands. Atmosphere, 14(4), 268-277.

Oke (1982). The energetic basis of the urban heat island. *Quarterly Journal of the Royal Meteorological Society*, 108, 1-24. https://doi.org/10.1002/qj.49710845502.

Oke, T. R., Mills, G., Christen, A., & Voogt, J. A. (2017). Urban Climates, pp. 520, Cambridge University Press, U.K.

Oleson K. W., Bonan, G. B., Feddema, J., & Jackson, T. (2011). An examination of urban heat island characteristics in a global climate model. *International Journal of Climatology*, 31, 1848-1865. https://doi.org/10.1002/joc.2201.

Pagowski, M. (2004). Some comments on PBL parameterizations in WRF. In The Joint WRF/MM5 Users' Workshop, Boulder, CO (Vol. 1, No. 9).

Riemann-Campe, K., Fraedrich, K., & Lunkeit, F. (2009). Global climatology of convective available potential energy (CAPE) and convective inhibition (CIN) in ERA-40 reanalysis. *Atmospheric Research*, *93*(1), 534-545. https://doi.org/10.1016/j.atmosres.2008.09.037.

Sailor, D.J., Elley, T.B., & Gibson, M. (2011). Exploring the building energy impacts of green roof design decisions – a modeling study of buildings in four distinct climates. *Journal of Building Physics*, 35(4), 372-391. https://doi.org/10.1177/1744259111420076.

Santamouris, M. (2014). Cooling the cities – A review of reflective and green roof mitigation technologies to fight heat island and improve comfort in urban environments. *Solar Energy*, 103, 682-703. https://doi.org/10.1016/j.solener.2012.07.003.

Shin, H. H., & Hong, S. Y. (2011). Intercomparison of planetary boundary-layer parametrizations in the WRF model for a single day from CASES-99. *Boundary-Layer Meteorology*, 139(2), 261-281. https://doi.org/10.1007/s10546-010-9583-z.

Sharma, A., Conry, P., Fernando, H. J. S., Hamlet, A. F., Hellmann, J. J., & Chen, F. (2016). Green and cool roofs to mitigate urban heat island effects in the Chicago metropolitan area: evaluation with a regional climate model. *Environmental Research Letters*, 11, 064004. https://doi.org/10.1088/1748-9326/11/6/064004.

Shashua-Bar, L., Pearlmutter, D., & Erell, E. (2011). The influence of trees and grass on outdoor thermal comfort in a hot-arid environment. *International Journal of Climatology*, 31(10), 1498-1506. https://doi.org/10.1002/joc.2177.

Simpson, J. R., & McPherson, E. G. (1997). The effects of roof albedo modification on cooling loads of scale model residences in Tucson, Arizona. *Energy and Buildings*, 25, 127-137. https://doi.org/10.1016/S0378-7788(96)01002-X.

Song, J., & Wang, Z. -H. (2015). Interfacing the urban land-atmosphere system through coupled urban canopy and atmospheric models. *Boundary-Layer Meteorology*, 154, 427-48. https://doi.org/10.1007/s10546-014-9980-9.

Song, J., & Wang, Z. -H. (2016). Diurnal changes in urban boundary layer environment induced by urban greening. *Environmental Research Letters*, 11, 114018. https://doi.org/10.1088/1748-9326/11/11/114018.

Song, J., Wang, Z. -H., Myint, S. W., & Wang, C. (2017). The hysteresis effect on surface-air temperature relationship and its implications to urban planning: An examination in Phoenix, Arizona, USA. *Landscape and Urban Planning*, 167, 198-211. https://doi.org/10.1016/j.landurbplan.2017.06.024.

Solcerova, A., van de Ven, F., Wang, M., Rijsdijk, M., & van de Giesen, N. (2017). Do green roofs cool the air?. *Building and Environment*, 111, 249-255. https://doi.org/10.1016/j.buildenv.2016.10.021.

Stull, R. B. (1988). An Introduction to Boundary Layer Meteorology, pp. 666, Kluwer Acad., Dordrecht, Netherlands.

Takebayashi, H., & Moriyama, M. (2007). Surface heat budget on green roof and high reflection roof for mitigation of urban heat island. *Building and Environment*, *42*(8), 2971-2979. https://doi.org/10.1016/j.buildenv.2006.06.017.

Wang, C., Wang, C., Myint, S. W., & Wang, Z. -H. (2017). Landscape determinants of spatio-temporal patterns of aerosol optical depth in the two most polluted metropolitans in the United States. *Science of the Total Environment*, 609, 1556–1565. https://doi.org/10.1016/j.scitotenv.2017.07.273.

Wang, C., & Wang, Z. -H. (2017). Projecting population growth as a dynamic measure of regional urban warming. *Sustainable cities and society*, 32, 357-365. https://doi.org/10.1016/j.scs.2017.04.010.

Wang, C., Myint, S. W., Wang, Z. -H., & Song, J. (2016). Spatio-temporal modeling of the urban heat island in the Phoenix Metropolitan Area: Land use change implications. *Remote Sensing*, 8, 185. https://doi.org/10.3390/rs8030185.

Wang, Z.-H., Bou-zeid, E., & Smith, J. A. (2013). A coupled energy transport and hydrological model for urban canopies evaluated using a wireless sensor network. *Quarterly Journal of the Royal Meteorological Society*, *139*(675), 1643-1657. https://doi.org/10.1002/qj.2032.

Washington, W. M., & Parkinson, C. (2005). Introduction to three-dimensional climate modeling. University science books.

Yang, J., Wang, Z. -H., Chen, F., Miao, S., Tewari, M., Voogt, J. A., & Myint S. (2015). Enhancing hydrologic modelling in the coupled Weather Research and Forecasting-urban modelling system. *Boundary-Layer Meteorology*, 155(1), 87-109. https://doi.org/10.1007/s10546-014-9991-6.

Yang, J., Wang, Z. -H., Georgescu, M., Chen, F., & Tewari M. (2016). Assessing the impact of enhanced hydrological processes on urban hydrometeorology with application to two cities in contrasting climates. *Journal of Hydrometeorology*, 17(4), 1031-1047. https://doi.org/10.1175/JHM-D-15-0112.1.

Yang, J., & Wang, Z. -H. (2017). Planning for a sustainable desert city: The potential water buffering capacity of urban green infrastructure. *Landscape and Urban Planning*, 167, 339-347. https://doi.org/10.1016/j.landurbplan.2017.07.014.

Yang, L., Smith, J. A., Baeck, M. L., Bou-Zeid, E., Jessup, S. M., Tian, F., & Hu H. (2014). Impact of urbanization on heavy convective precipitation under strong large-scale forcing: A case study over the Milwaukee–Lake Michigan region. *Journal of Hydrometeorology*, 15(1), 261-278. https://doi.org/10.1175/JHM-D-13-020.1.

Zhang, C. L., Chen, F., Miao, S. G., Li, Q. C., Xia, X. A., & Xuan, C. Y. (2009). Impacts of urban expansion and future green planting on summer precipitation in the Beijing metropolitan area. *Journal of Geophysical Research: Atmospheres*, 114, D2. https://doi.org/10.1029/2008JD010328.

Zhang, G. J. (2009). Effects of entrainment on convective available potential energy and closure assumptions in convection parameterization. *Journal of Geophysical Research: Atmospheres*, 114, D7. https://doi.org/10.1029/2008JD010976.

Table 1. Urban parameters of Phoenix metropolitan area used in the WRF simulation

Urban category	Commercial	High-density residential	Low-density residential
Building height (m)	10 [a]	7.5 [a]	5 [a]
Standard deviation of building height (m)	4 [a]	3 [a]	1 [a]
Roof width (m)	10 [a]	9.4 [a]	8.3 [a]
Road width (m)	10 [a]	9.4 [a]	8.3 [a]
Urban fraction (-)	0.865 [b]	0.609 [b]	0.569 [b]
Heat capacity of roof (MJ m^{-3} K^{-1})	1.7 [c]	1.7 [c]	1.7 [c]
Heat capacity of wall (MJ m^{-3} K^{-1})	1.7 [c]	1.7 [c]	1.7 [c]
Heat capacity of road (MJ m^{-3} K^{-1})	1.8 [c]	1.8 [c]	1.8 [c]
Thermal conductivity of roof (W m^{-1} K^{-1})	0.695 [c]	0.695 [c]	0.695 [c]
Thermal conductivity of wall (W m^{-1} K^{-1})	0.695 [c]	0.695 [c]	0.695 [c]
Thermal conductivity of road (W m^{-1} K^{-1})	0.4004 [a]	0.4004 [a]	0.4004 [a]
Surface albedo of conventional roof (-)	0.20 [a]	0.20 [a]	0.20 [a]
Surface albedo of green roof (-)	0.20 [d]	0.20 [d]	0.20 [d]
Surface albedo of white roof (-)	0.60 [d]	0.60 [d]	0.60 [d]
Surface albedo of wall (-)	0.20 [a]	0.20 [a]	0.20 [a]
Surface albedo of road (-)	0.15 [c]	0.15 [c]	0.15 [c]
Surface emissivity of roof (-)	0.90 [a]	0.90 [a]	0.90 [a]
Surface emissivity of wall (-)	0.90 [a]	0.90 [a]	0.90 [a]
Surface emissivity of road (-)	0.95 [a]	0.95 [a]	0.95 [a]
Roughness length for momentum over roof (m)	0.01 [a]	0.01 [a]	0.01 [a]
Roughness length for momentum over wall (m)	0.0001 [a]	0.0001 [a]	0.0001 [a]
Roughness length for momentum over road (m)	0.01 [a]	0.01 [a]	0.01 [a]

a. Default values prescribed in WRF-SLUCM scheme and can be found in Chen et al. (2011)

b. Myint et al. (2011), Chow et al. (2014)

c. Calibrated parameters based on Yang et al. (2015), Song and Wang (2015)

d. Prescribed values for designed scenarios in this paper

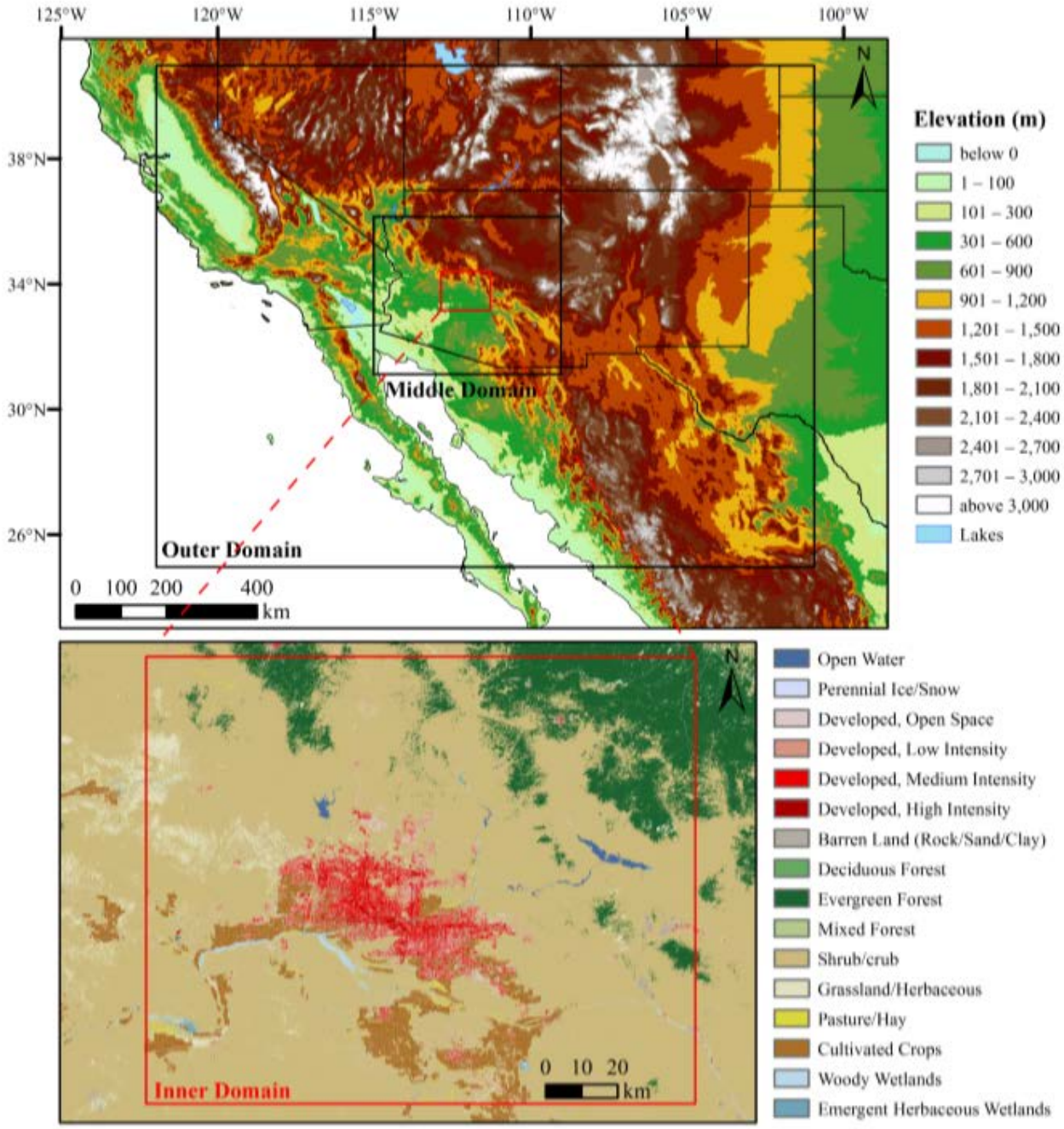

Figure 1. (a) Geographical representations of the 3 model domains (outer, middle, inner) with the overlaid topography, and (b) the NLCD land cover map for the inner domain.

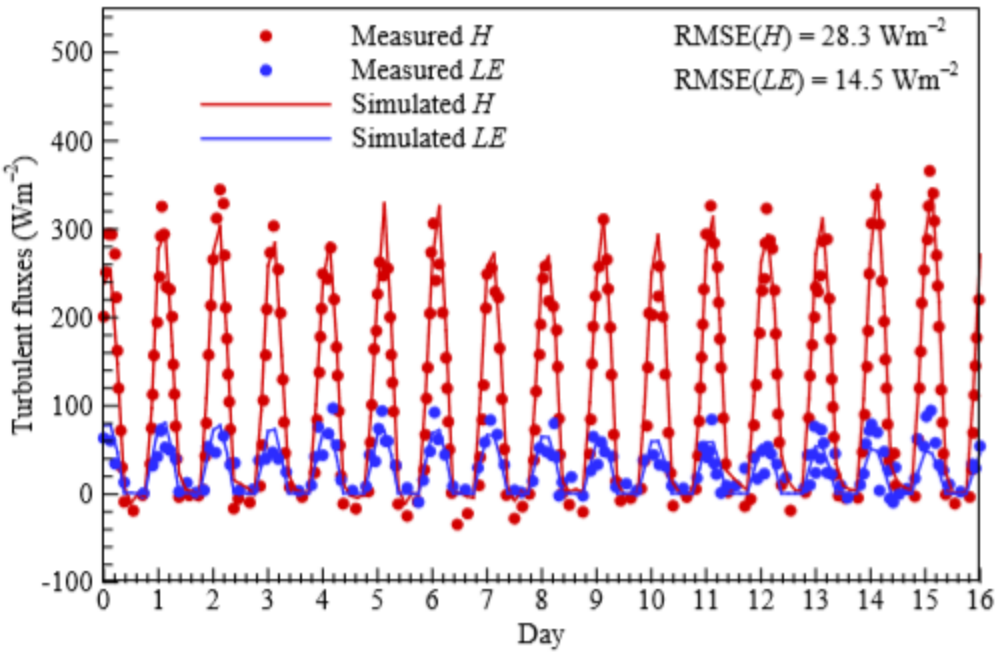

Figure 2. Comparison of field measurements against model simulation results of urban surface turbulent sensible (*H*) and latent (*LE*) fluxes from 13 June 2012 11:00 to 29 June 2012 11:00 (Local time) at west Phoenix site.

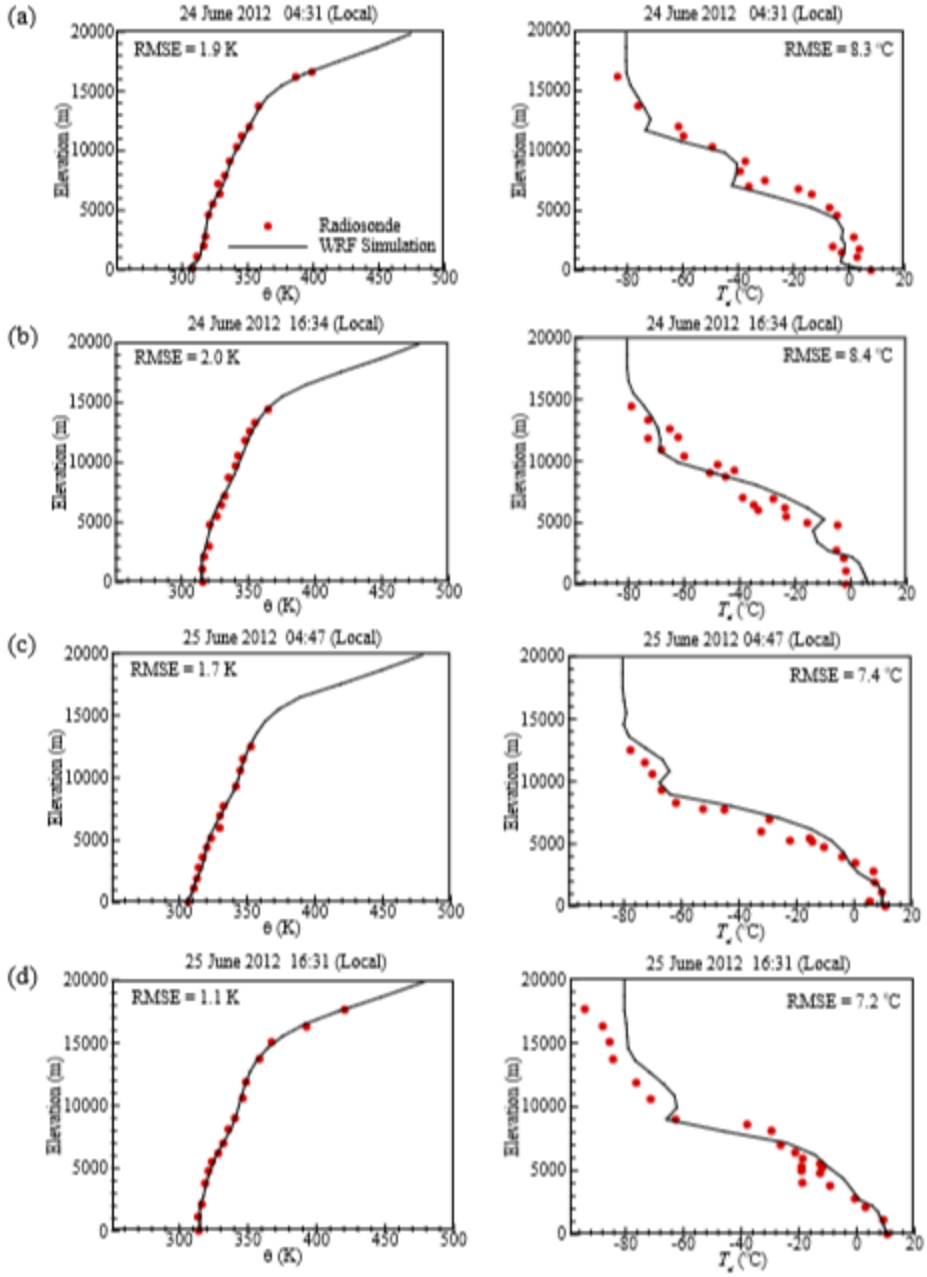

Figure 3. Comparison of field measurements against model simulation results for profiles of potential temperature (θ) and dewpoint temperature (T_d) at 4 different time instants: (a) 04:31 on

24 June 2012, (b) 16:34 on 24 June 2012, (c) 04:47 on 25 June 2012, and (d) 16:31 on 25 June 2012 (all in local time) at east Phoenix site.

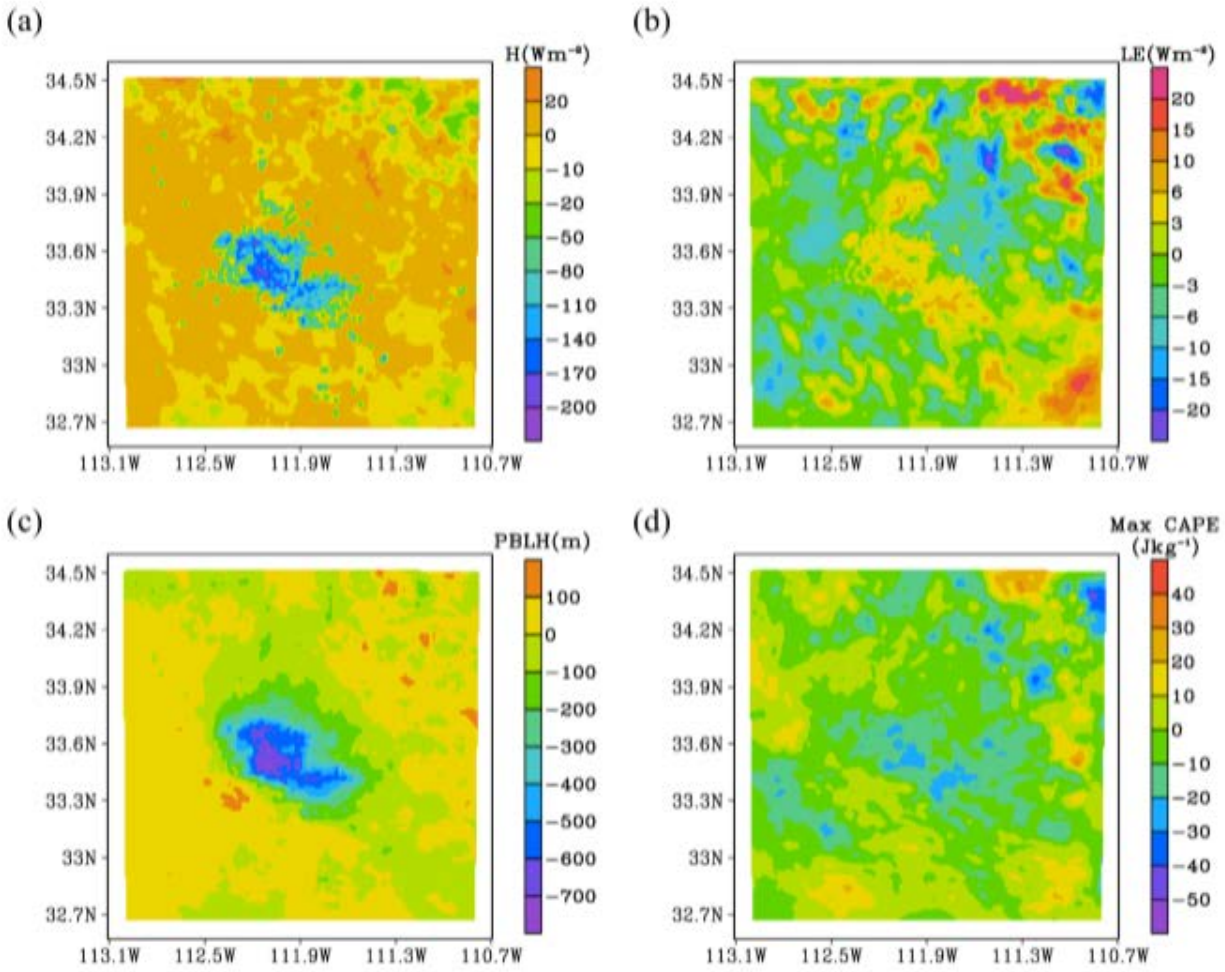

Figure 4. The differences of (a) sensible heat flux (*H*), (b) latent heat flux (*LE*), (c) PBL height (PBLH) and (d) maximum CAPE between the green roof scenario and the control scenario averaged over the three summer months (JJA), sampled at 2 pm (local time).

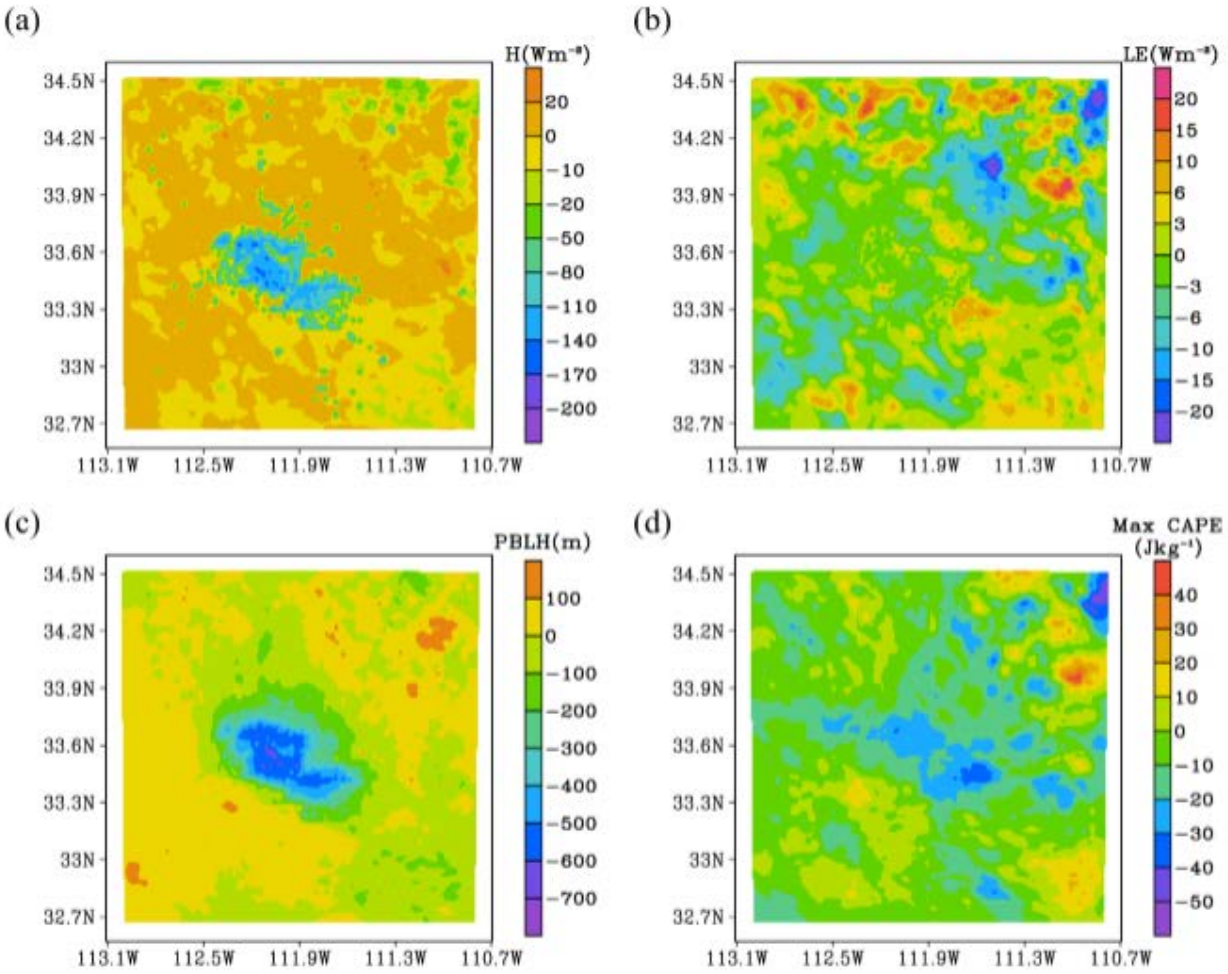

Figure 5. Same as Figure 4, but for the white roof scenario.

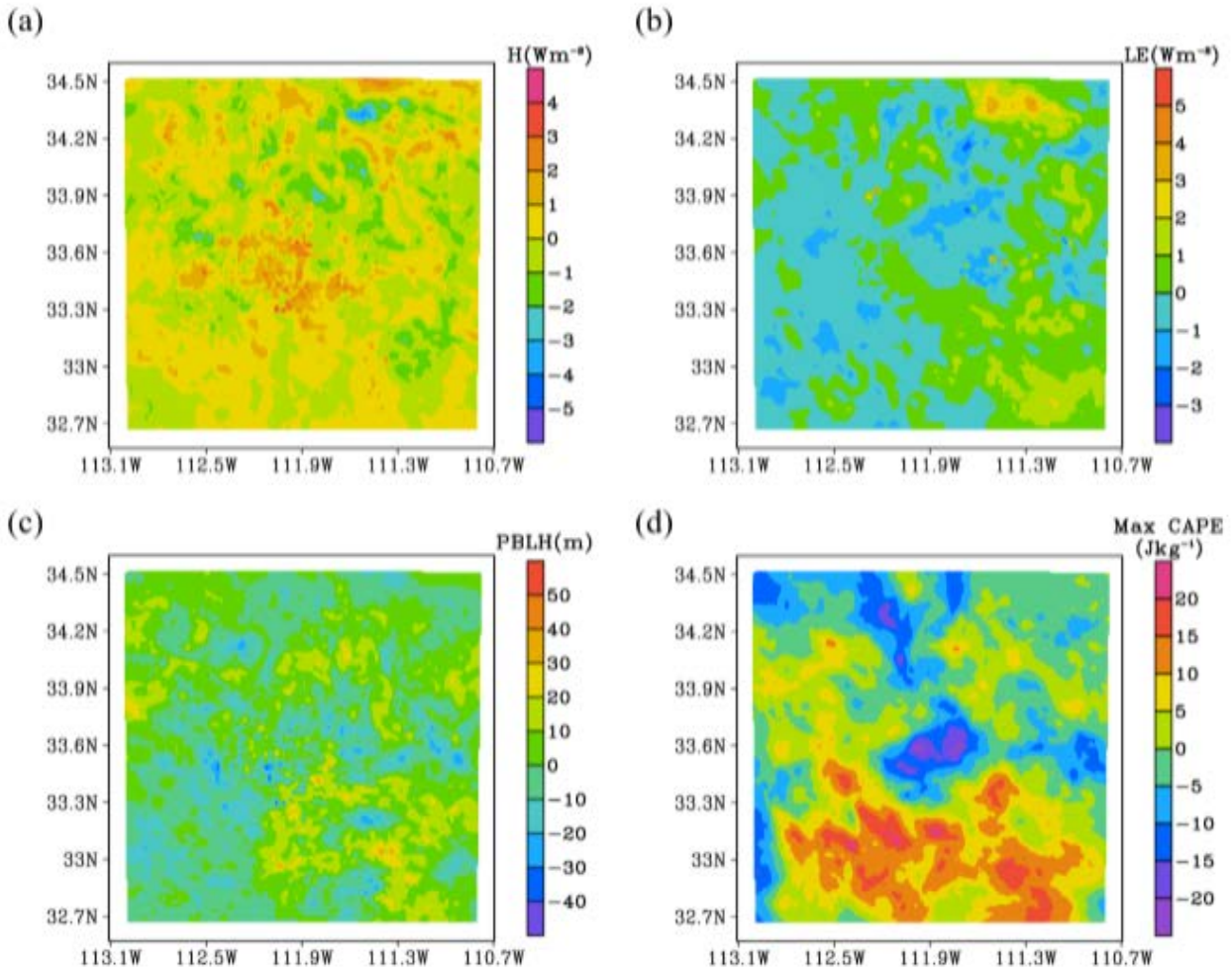

Figure 6. Same as Figure 4, but sampled at 2 am.

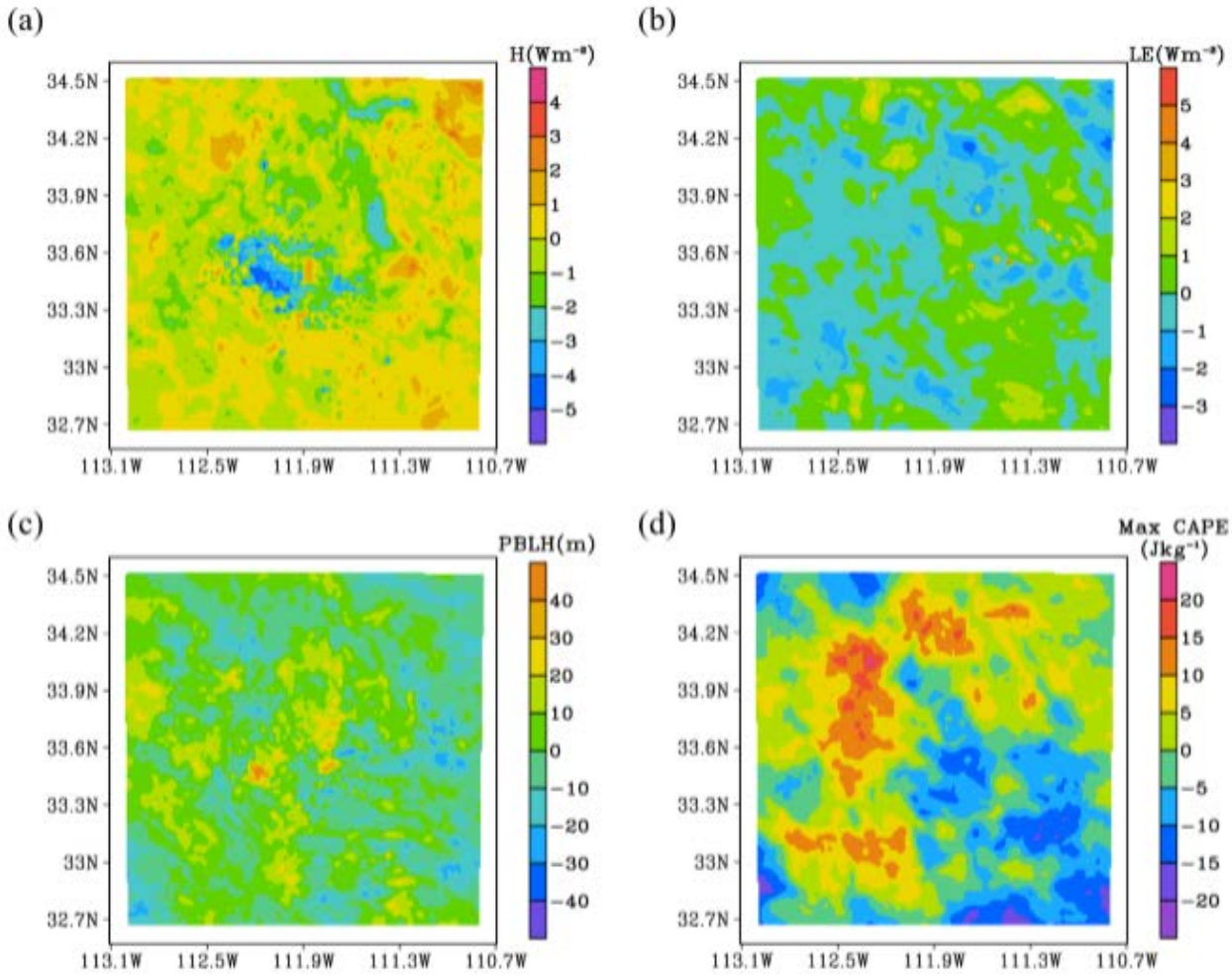

Figure 7. Same as Figure 5, but sampled at 2 am.

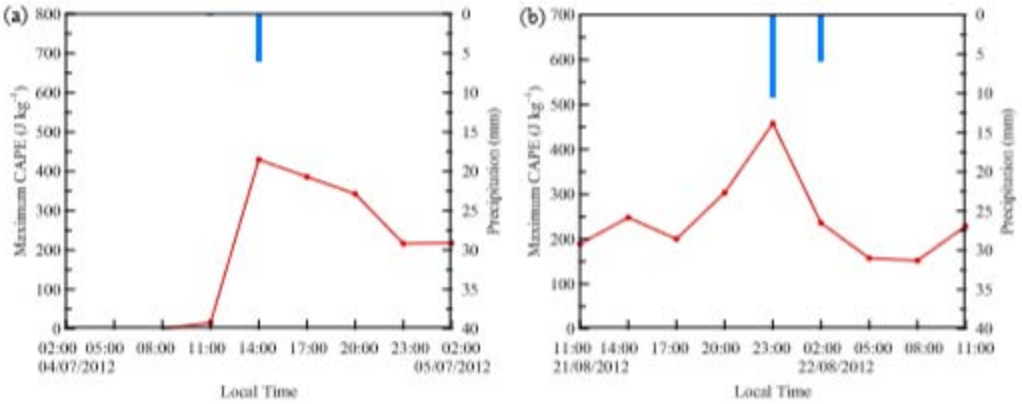

Figure 8. The time variation of 3-hourly maximum CAPE in 24 hours among which rainfall events occur at (a) daytime and (b) nighttime. For consistency, the precipitation bar also shows the total 3-hourly precipitation amount.

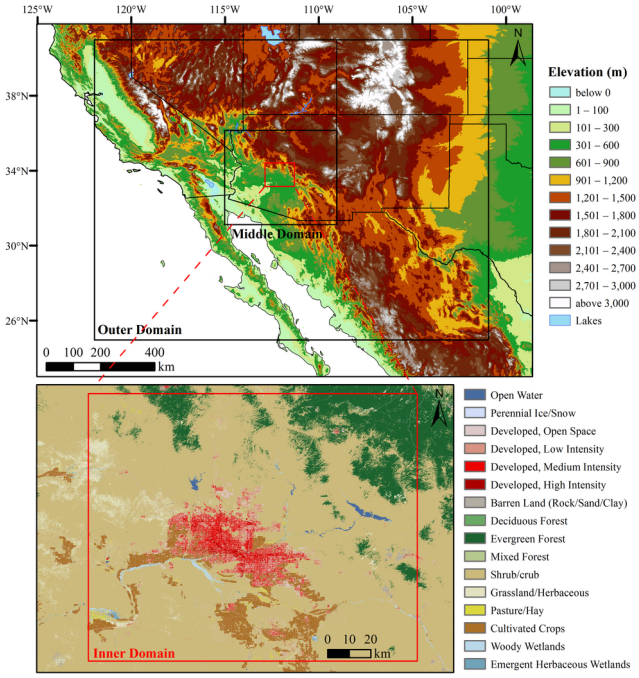

2018JD028302-f01-z-.tif

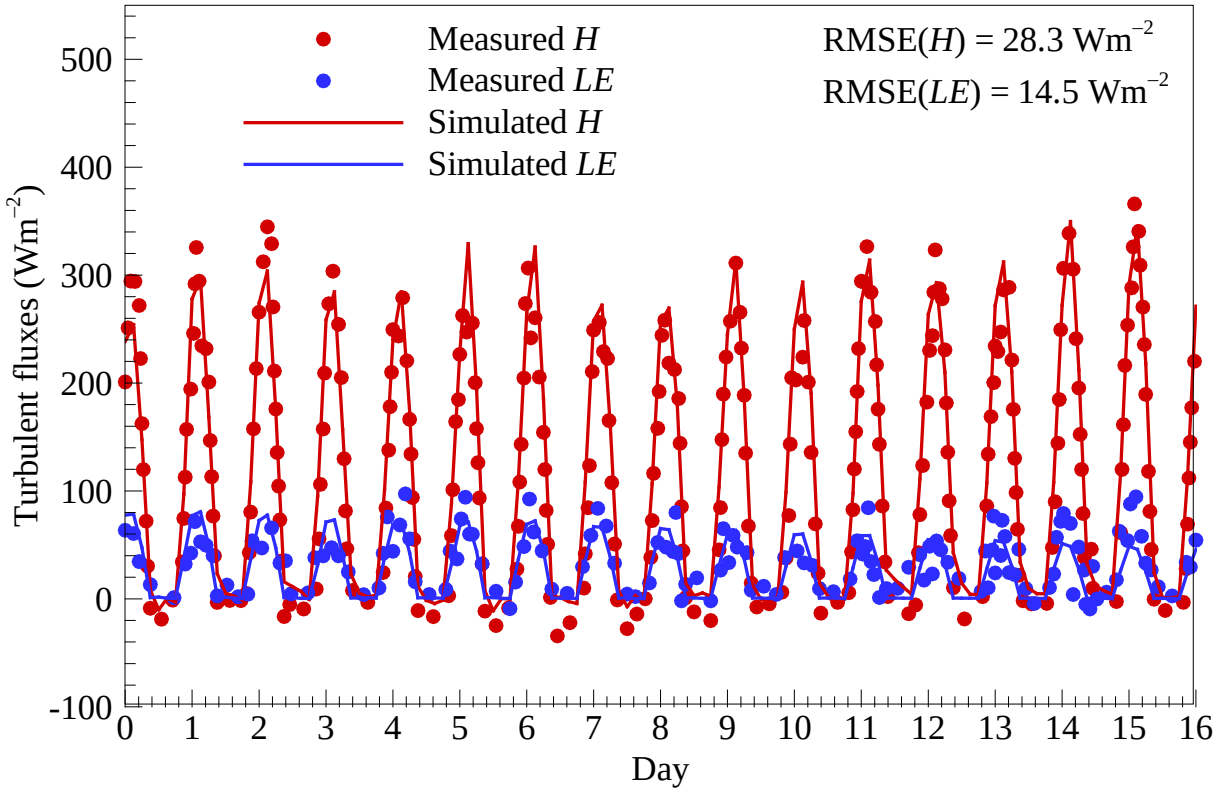

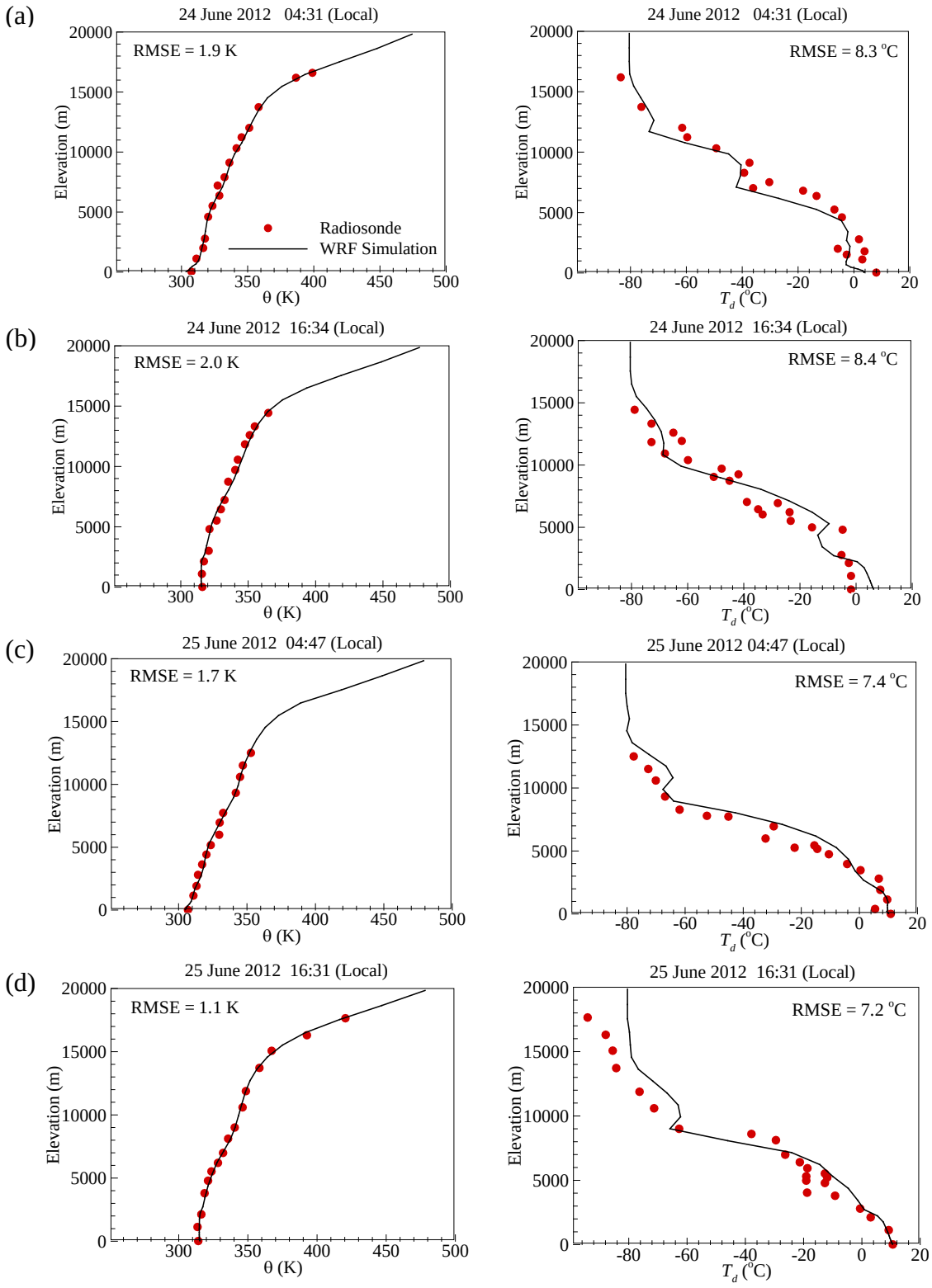

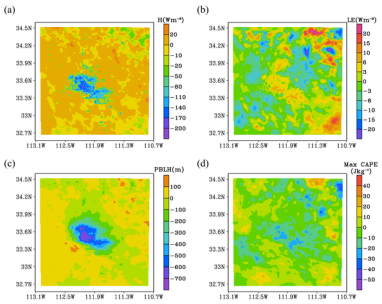

2018JD028302-f04-z-.tif

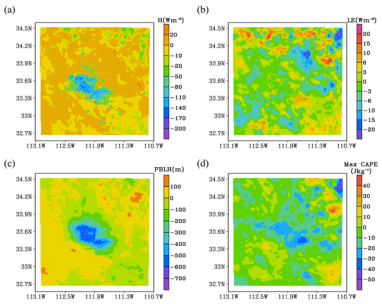

2018JD028302-f05-z-.tif

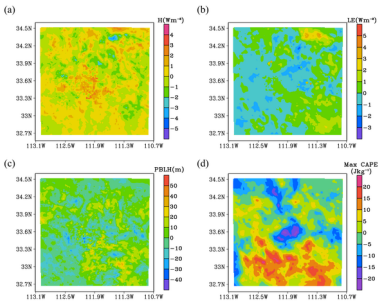

2018JD028302-f06-z-.tif

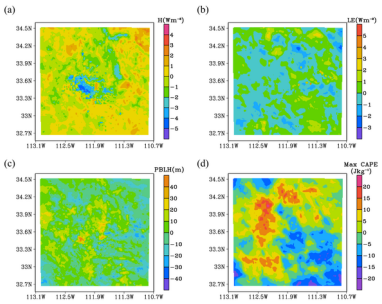

2018JD028302-f07-z-.tif

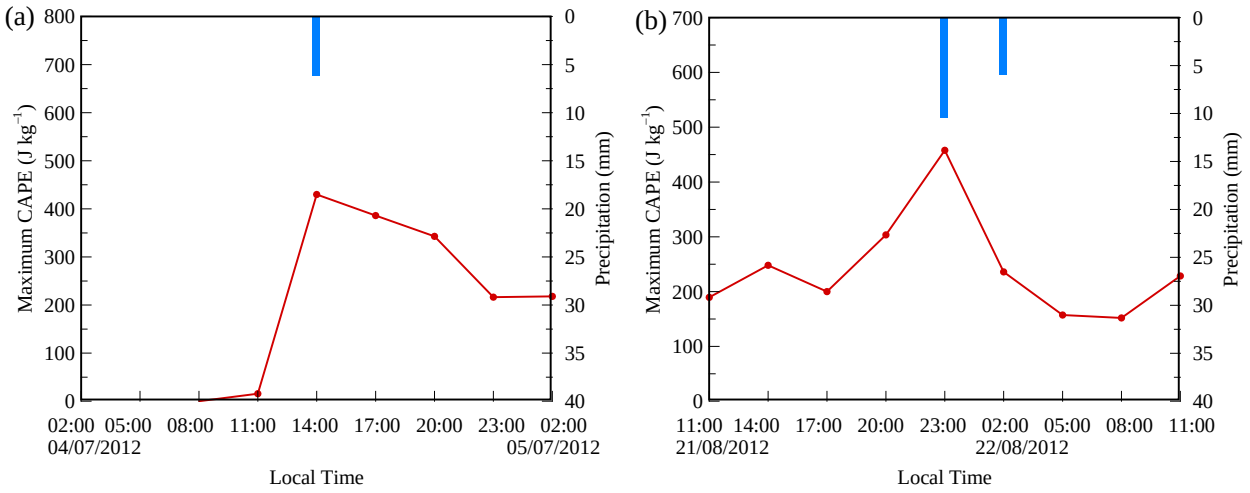

Table 1. Urban parameters of Phoenix metropolitan area used in the WRF simulation

Urban category	Commercial	High-density residential	Low-density residential
Building height (m)	10 [a]	7.5 [a]	5 [a]
Standard deviation of building height (m)	4 [a]	3 [a]	1 [a]
Roof width (m)	10 [a]	9.4 [a]	8.3 [a]
Road width (m)	10 [a]	9.4 [a]	8.3 [a]
Urban fraction (-)	0.865 [b]	0.609 [b]	0.569 [b]
Heat capacity of roof (MJ m^{-3} K^{-1})	1.7 [c]	1.7 [c]	1.7 [c]
Heat capacity of wall (MJ m^{-3} K^{-1})	1.7 [c]	1.7 [c]	1.7 [c]
Heat capacity of road (MJ m^{-3} K^{-1})	1.8 [c]	1.8 [c]	1.8 [c]
Thermal conductivity of roof (W m^{-1} K^{-1})	0.695 [c]	0.695 [c]	0.695 [c]
Thermal conductivity of wall (W m^{-1} K^{-1})	0.695 [c]	0.695 [c]	0.695 [c]
Thermal conductivity of road (W m^{-1} K^{-1})	0.4004 [a]	0.4004 [a]	0.4004 [a]
Surface albedo of conventional roof (-)	0.20 [a]	0.20 [a]	0.20 [a]
Surface albedo of green roof (-)	0.20 [d]	0.20 [d]	0.20 [d]
Surface albedo of white roof (-)	0.60 [d]	0.60 [d]	0.60 [d]
Surface albedo of wall (-)	0.20 [a]	0.20 [a]	0.20 [a]
Surface albedo of road (-)	0.15 [c]	0.15 [c]	0.15 [c]
Surface emissivity of roof (-)	0.90 [a]	0.90 [a]	0.90 [a]
Surface emissivity of wall (-)	0.90 [a]	0.90 [a]	0.90 [a]
Surface emissivity of road (-)	0.95 [a]	0.95 [a]	0.95 [a]
Roughness length for momentum over roof (m)	0.01 [a]	0.01 [a]	0.01 [a]
Roughness length for momentum over wall (m)	0.0001 [a]	0.0001 [a]	0.0001 [a]
Roughness length for momentum over road (m)	0.01 [a]	0.01 [a]	0.01 [a]

a. Default values prescribed in WRF-SLUCM scheme and can be found in Chen et al. (2011)

b. Myint et al. (2011), Chow et al. (2014)

c. Calibrated parameters based on Yang et al. (2015), Song and Wang (2015)

d. Prescribed values for designed scenarios in this paper